JOURNAL OF MATERIALS SCIENCE 18 (1983) 3288–3298

Relationship between microstructure, hardness and electrical conductivity of 2219 aluminium

M. NATAN
Martin Marietta Laboratories, Baltimore, Maryland 21227, USA

R. A. CHIHOSKI
Martin Marietta-Denver Aerospace, Denver, Colorado, USA

A TEM study of unstretched, heat-treated aluminium alloy 2219 was performed with the aim of correlating the microstructure with hardness (H) and eddy current conductivity (C) data. Recently Chihoski has developed a new method of evaluating heat treatments of aluminium alloys by constructing in an H–C field a "sail" formed by a network of curved coordinate lines of quenching and ageing times. In this paper it is shown that a pair of H–C values, as represented by a point in the "sail" is uniquely related to the microstructure. The hardness after quenching (zero ageing) depends on the amount of primary θ'- and θ-phases developed during quenching, and decreases with increased precipitate incoherency and size. Upon ageing at 190° C, H first increases due to precipitation of coherent zones and phases (e.g. GP(1) and θ''), then decreases after a $\theta'' \rightarrow \theta'$ transformation mainly due to changes in their relative population and, to a much lesser degree, due to loss of coherency in the θ'. The conductivity is mainly a function of the copper solute concentration in the matrix, and increases significantly only when copper is drained from the matrix to form θ' and θ. The study supports Chihoski's conclusion that construction of a "sail" for a given aluminium alloy provides a quick, nondestructive method for determination of precipitation processes, and can be very useful in quality control, failure analysis and metallurgical research.

1. Introduction

Some commerical aluminium alloys exhibit complex variations in both hardness and electrical conductivity as a function of heat treatment. The complex nature of the behaviour make it difficult, if not impossible, to use either measurement alone to characterize the nature of the heat treatment after the fact. However, in recent studies, Chihoski [1, 2] has shown that the combined H–C data serves as a sensitive indicator of the thermal history in 2219, the alloy studied. He used the H–C field to construct a "sail", Fig. 1, from experimental points obtained in various quench and ageing sequences. The sail is formed by a net of curved coordinate lines: increasing cooling times running from top (high H) to bottom (low H), and increasing ageing times running from right (low C) to left (high C). When the H–C values of a test specimen are inserted into the sail, its thermal history in terms of a quench and ageing sequence can be retroactively pinpointed with confidence.

This strong connection between the combined H–C data and the thermal history must be related to the unique microstructure that develops after each heat treatment. In this study we examine the microstructure of various points in the sail and discuss its relationship to hardness and conductivity.

2. Experimental methods

2.1. Materials

A single lot of 2219 aluminium alloy was solution

0022–2461/83 $03.00 + .12

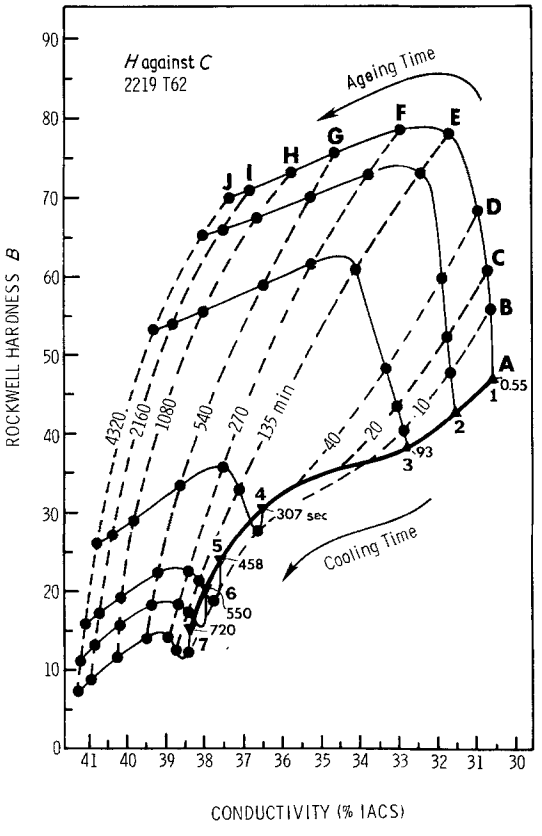

Figure 1 A "sail" in the *H–C* field constructed by plotting the *H–C* data after known quenching and ageing conditions.

treated at 530° C, then divided into parts which were quenched at seven different rates as described shortly. The lot composition is given in Table I.

After quenching, the material was held at room temperature for 96 h to bring it to the T42 condition. Conductivity and hardness measurements were started on the T42 material before any artificial ageing and marked "A".

The various heat treatments used are graphically illustrated in Fig. 2, where the numbers 1 through to 7 represent various quenching paths superimposed on the dashed lines of a nucleation diagram drawn after Hornbogen [3]. The quenching time was arbitrarily defined as the time needed to cool a specimen from 410 to 190° C and ranged from 0.55 to 720 sec. Panels were labelled accordingly 1 to 7. After 96 h at room temperature, specimens from each panel were aged at 190° C for various times labelled B to J in Fig. 1. Thus the thermal history of each specimen is defined by a number (quenching time) and a letter (ageing time). For example, specimen 1D was quenched in 0.55 sec and aged at 190° C for 40 min.

2.2. Electron microscopy

Thin foils for transmission electron microscopy (TEM) were prepared from each of the heat-treated samples. First a diamond saw at slow speed cut thin 0.2 mm slices, from which 3 mm diameter discs were punched out. The discs were electro-jet polished in a 30% HNO_3-methanol solution at below $-25°$ C, rinsed in methanol and stored under vacuum in a desiccator, at room temperature.

Observations were carried out in a JEM 100CX scanning transmission electron microscope, operating in the TEM mode at 100 kV. All selected area diffraction patterns (SADP) were taken with the specimen tilted, using a double tilt holder, to an exact ⟨0 0 1⟩ zone. Bright-field micrographs were taken with two-beam conditions using a low index {2 0 0} reflection close to the ⟨0 0 1⟩ zone, which insures consistency in the contrast and allows a systematic comparison of the various microstructures. Diffraction patterns were taken with a 20 μm diffraction aperture at a magnification of 50 K in the selected area diffraction mode, thereby providing a certain consistency in the contribution of various precipitate phases to the diffraction pattern. Since the choice of area viewed is arbitrary, we made an effort to present microstructures that are typical.

3. Results

The TEM results are grouped for convenience as three separate figures: low magnification micrographs (Fig. 3a), high magnification micrographs (Fig. 3b) and SAD patterns (Fig. 4). The presentation is coordinated for all three, with the microstructure of each specimen being discussed in terms of precipitate phases seen in Figs. 3a and b, finer details from Fig. 3b, and precipitate coherency from Figs. 3b and 4. Each specimen is identified by the convention mentioned in Section 2.1.

The following summarizes the observations made in the study of panel 1 as it was aged from

TABLE I Composition of 2219 aluminium alloy in study

Element	Cu	Mn	Fe	Si	Mg	Zn	Ti	V	Zr	Other
wt%	5.80	0.21	0.13	0.04	0.01	0.05	0.01	0.07	0.14	< 0.15

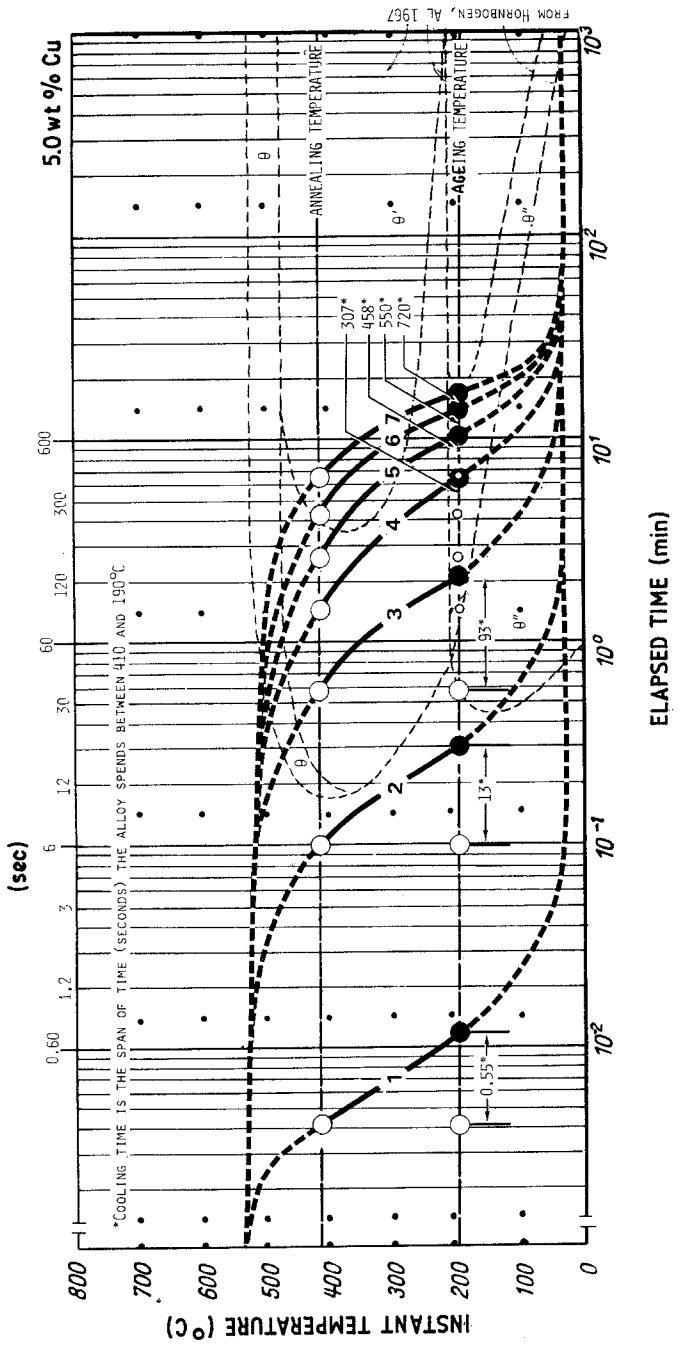

Figure 2 Schematics of heat treatments superimposed on a nucleation diagram after Hornbogen [3].

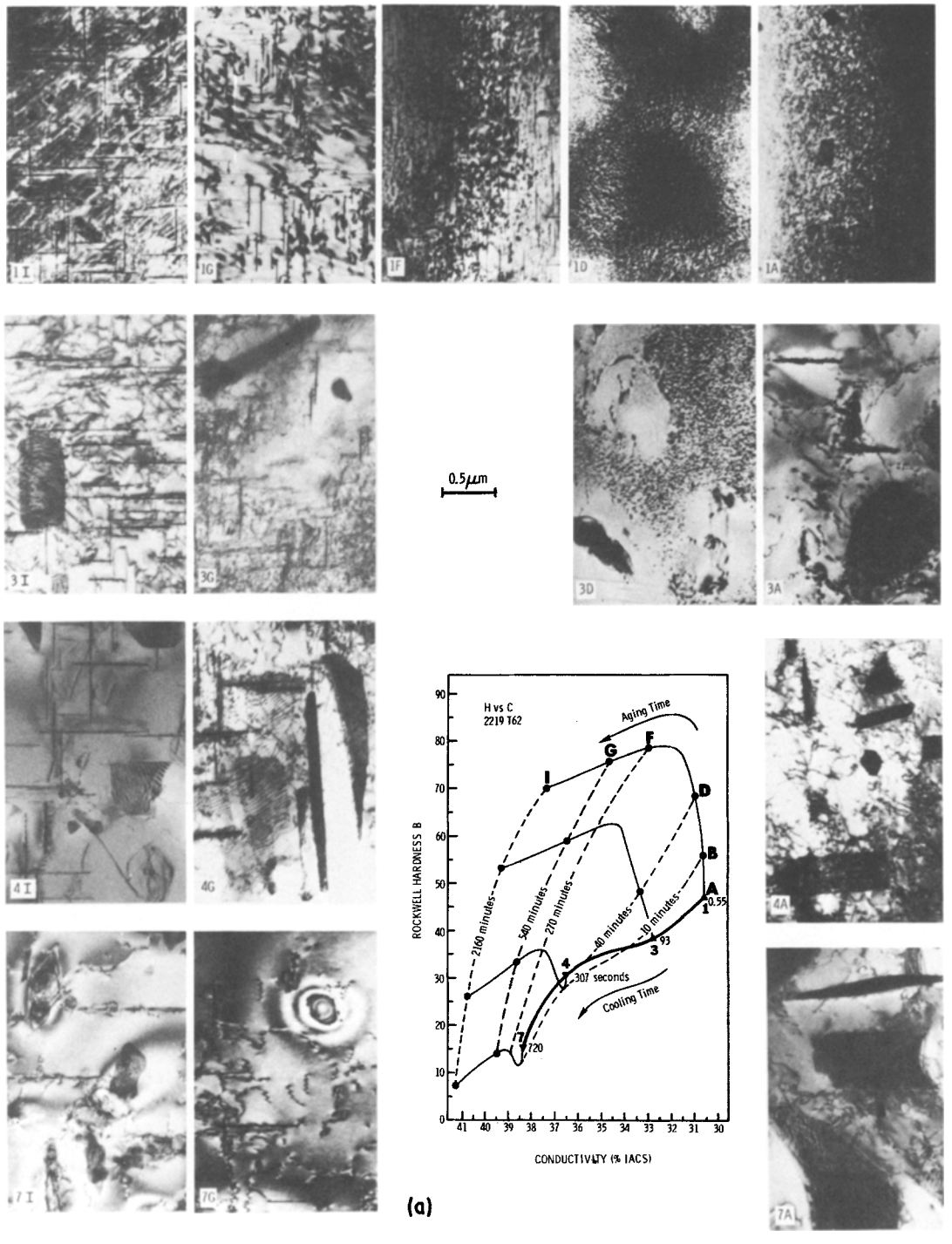

Figure 3 (a) Low magnification TEM micrographs of microstructures at various points in the sail. Taken with a two beam condition close to a ⟨0 0 1⟩ zone. (b) High magnification of typical areas.

status A (0 min) through D, F, G and finally I (2160 min). The microstructures are shown in Fig. 3, photos 1A through 1I. In 1A there is a uniform structure lacking sharp detail. The corresponding SADP (Fig. 4) however shows faint streaks emanating from strong {2 0 0} α-Al matrix reflections in the ⟨1 0 0⟩ directions and thus indicates the start of precipitation, most likely of GP(1) zones. According to previous studies [4, 5] these zones precipitate as discs of about 5.0 nm

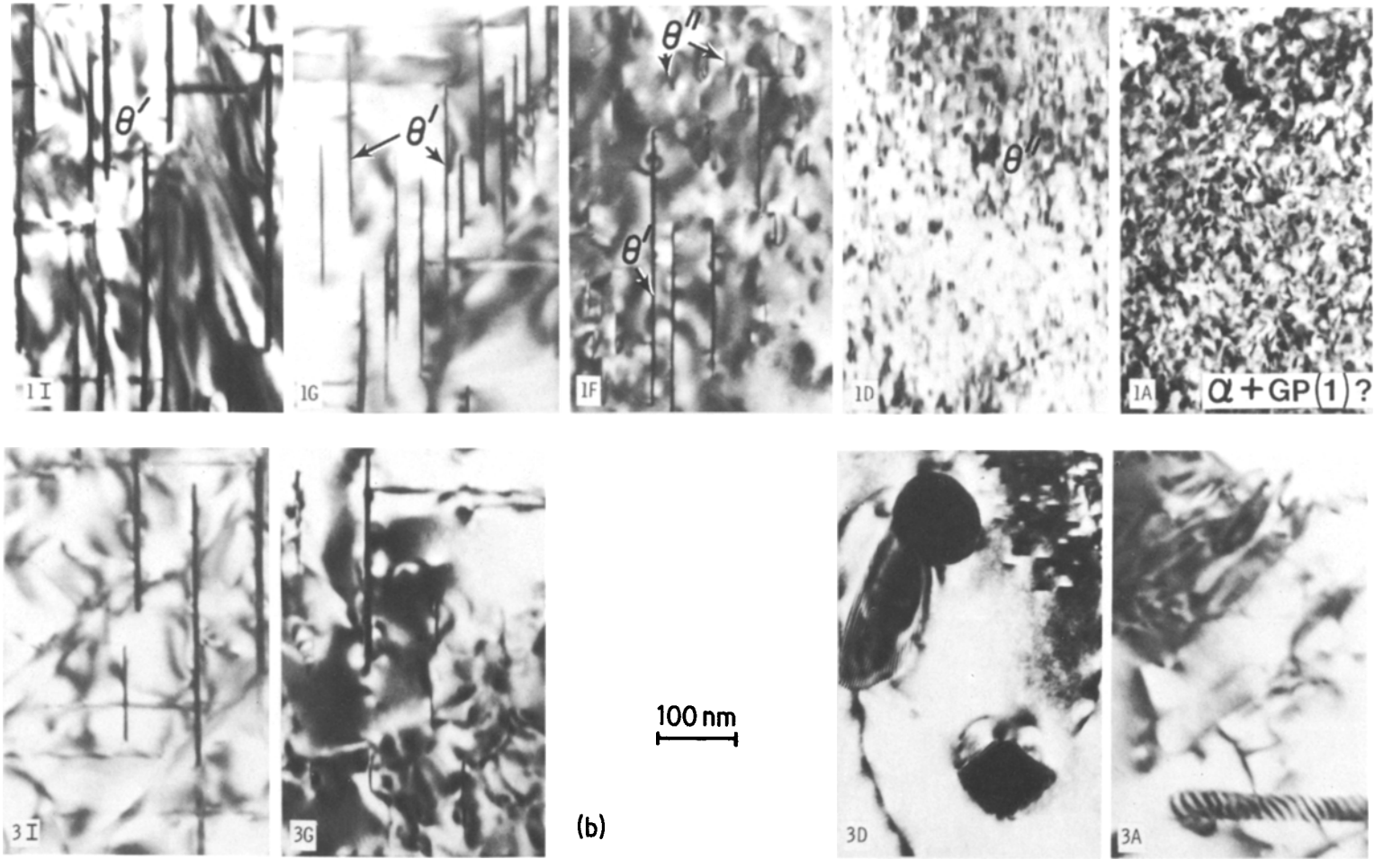

Figure 3 Continued.

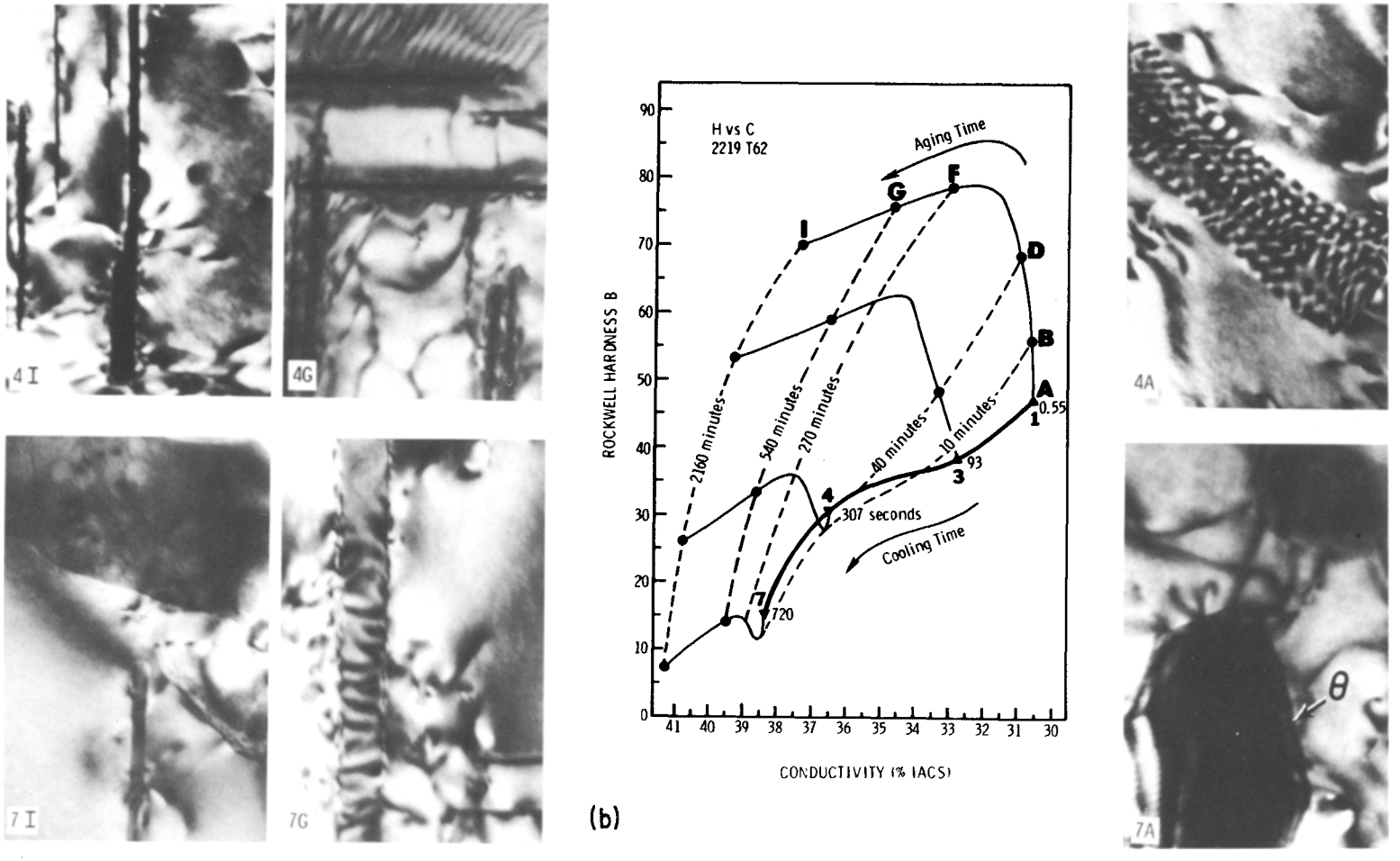

Figure 3 (b) Continued.

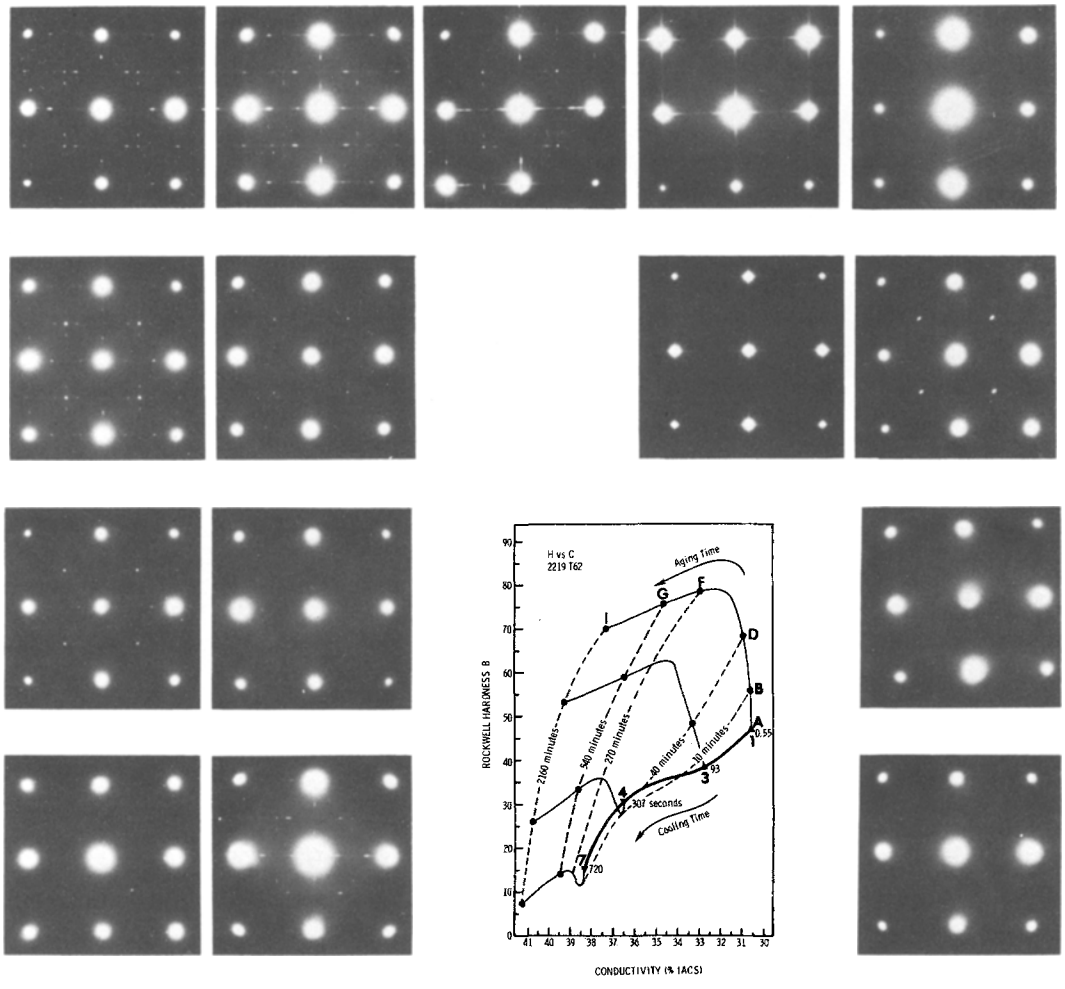

Figure 4 Selected area diffraction patterns at various points in the sail. Taken with a 20 μm SAD aperture at an exact ⟨0 0 1⟩ zone axis.

diameter and 1 to 2 atomic layers thickness on {1 0 0} planes. They are coherent and introduce strains in the matrix which lead to streaking in the SADP and to strain contrast in bright-field views. Individual zones were first observed by us at 1B (not shown). With additional annealing, they grew so that in 1D, Figs. 3a and b, thin precipitates, about 20 to 30 nm in diameter and 1.5 to 2.5 nm thick are seen laying on two {1 0 0} habit planes perpendicular to the foil surface. We will follow previous authors [4, 6] and assume that they belong to a distinctly new phase, θ'', although according to Phillips [7], the transformation from GP(1) to θ'' is gradual and any distinction is arbitrarily based on size. The θ'' precipitates are also fully coherent with the matrix. A few, small, block-like inclusions seen at low magnification in sequence 1 may be due to various additives in the 2219 aluminium alloy. Precipitates such as Cu_2FeAl_7 and $Cu_2Mn_3Al_{20}$ are likely to appear in the microstructure [8], but do not significantly affect the precipitation aspects discussed here.

Specimen 1F exhibits two kinds of precipitates that share the {1 0 0} habit planes: smaller ones similar to those in 1D (θ''), and larger ones identified by the SADP reflections and by their size [6–12] as θ'. Most of the reflections in the SADP are common to both θ'' and θ', and a very careful analysis is needed to separate them [8, 12]. The development of various phases around the *HC* reversal region (1E to 1F) on locus 1, Fig. 1, can be followed on the SAD patterns, two of which are also shown separately in Fig. 5. Before 1F (e.g. 1D), the SADP includes matrix {2 0 0} reflections, ⟨1 0 0⟩ streaks passing through them,

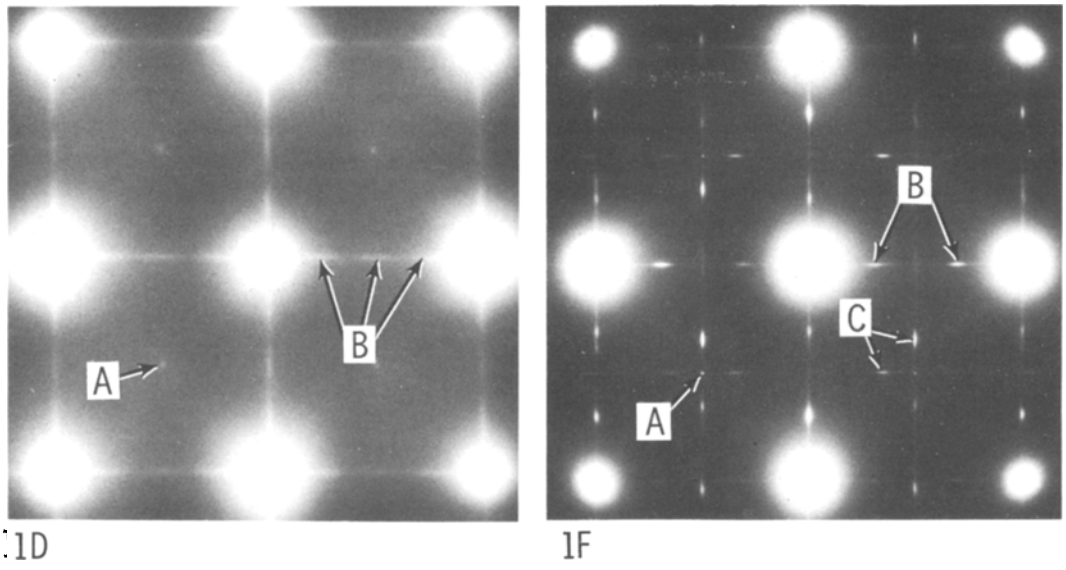

Figure 5 Selected area diffraction patterns of 1D and 1F showing the following: 1F – faint spots at {1 1 0} matrix positions due to the start of θ' precipitation on {1 0 0} planes parallel to the foil surface (A), and streaks passing through {2 0 0} matrix reflections and just starting to develop maxima due to coherent precipitation (B). 1D – same details as in 1F plus streaking and developed maxima through {1 1 0} matrix positions (C) due to the new θ'-phase precipitating on two {1 0 0} habit planes perpendicular to the foil surface.

and faint spots at {1 1 0} matrix positions. The streaks, which were continuous in 1A and 1B start to develop maxima around 1D, a phenomenon first observed in pure Al–Cu alloys by Guinier [6] and more recently in 2219 alloy by Papazian [12] and which is generally attributed to the formation of a distinct new phase – θ''. Alternatively, Phillips [7] interpreted it as due to the formation of multilayer copper rich regions in an otherwise continuous development process of the GP zones. According to Phillips, faint spots at {1 1 0} positions are attributable to θ' platelets laying in the {1 0 0} plane parallel to the foil surface, which are too thin and sparse to be seen in the microstructure. Our observations tend to confirm that before the *HC* reversal the dominant phase is θ'' and that although precipitation of θ' commences very close to it (i.e. 1D) its amount is negligible and hard to detect by TEM.

After further ageing to 1F the SADP, Fig. 5, shows all the reflections seen in 1D, but with much stronger and distinct maxima in the streaks. In addition, it shows streaks through the {1 1 0} matrix positions, parallel to ⟨1 0 0⟩ matrix directions. These streaks, which first appear and are fairly continuous at the *HC* reversal, (point 1E, not shown), break up in 1F and start to develop maxima corresponding to {1 1 0}-type reflections for two θ' sets of platelets oriented perpendicular to the foil surface, as reported for pure Al–Cu alloys by Phillips [7] and for 2219 aluminium alloy by Papazian [12]. Strain contrast is evident in all micrographs, indicating, in accord with the remaining streaks in the SADP, that some degree of coherency is retained in the precipitates.

Upon further ageing Fig. 3 shows that the microstructure in 1G is similar to that in 1F except that significantly fewer small θ'' precipitates are visible alongside bigger θ'. This condition is due to a continuing process of $\theta'' \rightarrow \theta'$ transformation in which the θ'' dissolve and provide copper to the growing θ'. This transformation advances so that in 1I the predominant precipitate phase is θ'. The θ' discs or plates are still quite uniform, but slightly longer and thicker than in 1F or 1C. Their density seems somewhat less than in 1F and it is possible that some θ' dissolution occurs simultaneously with θ' coarsening. It has been pointed out by others [11] that formation of the stable θ-$CuAl_2$ phase is not expected at 190° C ageing and indeed θ was not observed on locus 1. The overageing condition represented by the drop in H after the reversal point is frequently ascribed to a loss of coherency in the main precipitate phase (e.g. Rosen *et al.* [13]). However, as the θ' precipitates in 1I do not exhibit any

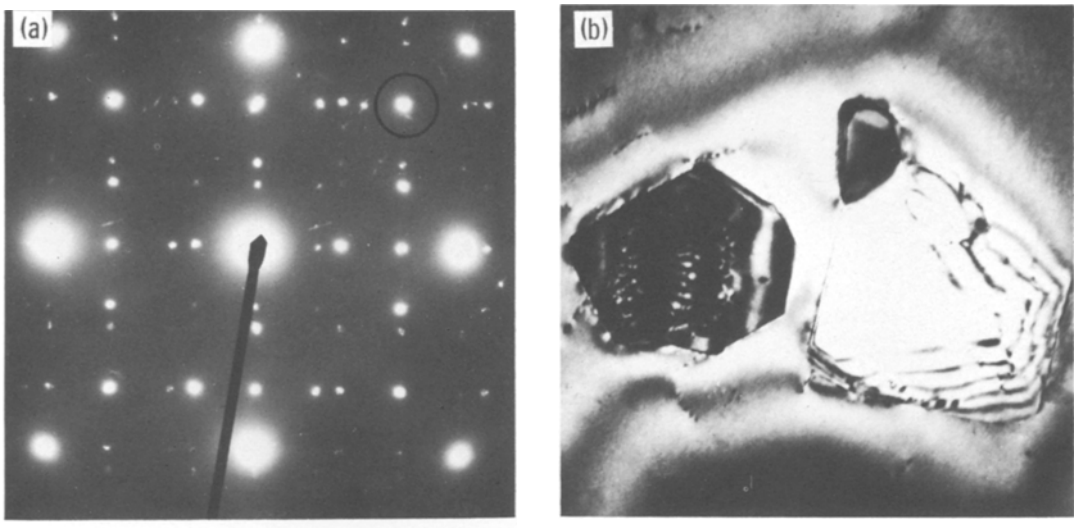

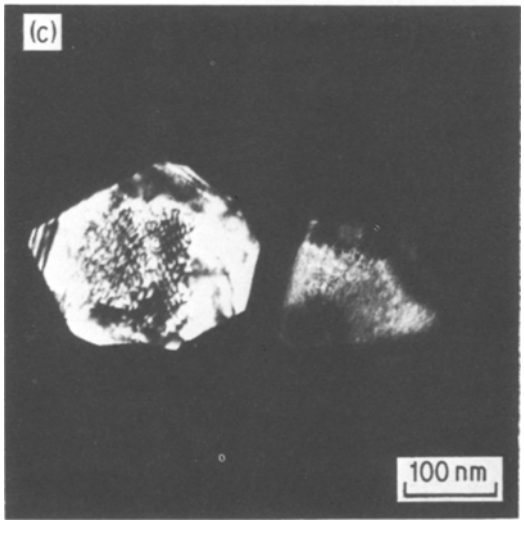

Figure 6 Bright field (a), dark field (b), and SADP views (c), of a θ precipitate typical to microstructures on locus 4. The dark field view was taken with the circled reflection tentatively identified as $(2\,2\,0)_\theta$. Note that similar precipitate reflections were not observed on locus 1.

interface dislocations, and their thickness of < 15.0 nm is much smaller than that associated with loss of coherency [10], we conclude that the θ' remains coherent on locus 1, and the H drop must be due to other factors, as discussed later.

Although the possible precipitate phases in a commercial alloy such as 2219 are more numerous and complex than those in its closest binary Cu–Al counterpart [8], in general the precipitation sequence expected upon ageing remains: supersaturated $\alpha \rightarrow \mathrm{GP}(1) \rightarrow \theta'' \rightarrow \theta' \rightarrow \theta$. It is also expected that increasing cooling times, or holding periods at elevated temperatures, such as occur in the time traces 1 to 7 in Fig. 2 would allow a "primary" precipitation of θ' and possibly θ during cooling, prior to ageing. That this indeed is the case is shown in Fig. 3. In 3A, we mostly see θ' precipitates, both parallel and perpendicular to the foil surface. The parallel ones have misfit dislocations on their broad surfaces, i.e. are incoherent, and lead to $\{1\,1\,0\}$ reflections in the SADP. The perpendicular ones are too few to cause visible streaking and maxima in the SADP. Some dislocations probably were introduced during foil preparation.

The observations down the A locus of Fig. 1 mark a different kind of change in status, as the quenching time associated with each panel is larger. In 4A (Fig. 3) the θ' precipitates have various shapes and sizes and some exhibit extensive networks of misfit dislocations. θ precipitates appear in increasing numbers and can be identified mainly from additional reflections in the SADP, Fig. 6, reflections which never appear at any of the points on locus 1. The θ' also broaden and thicken with slower quenches and those on the $\{1\,0\,0\}$ planes parallel to the surface exhibit stronger contrast and extensive networks of interface dislocations. Slower quenches cause therefore precipitation of "primary" θ' and θ as well as coarsening and loss of coherency of the θ'.

The ageing performed after quenching allows phase transformations in parallel to those on locus 1 to also occur in loci 3 through to 7. However, a major difference in the precipitation processes is caused by the amount of existing primary

θ' and θ phases. Both phases drain copper solute from the matrix leading to denuded zones around the precipitates. Such zones are especially evident in 3D, Figs. 3a and b, where a fine θ'' phase appears everywhere except near the primary θ' precipitates. Longer ageing leads to θ'' dissolution and additional secondary θ' formation as seen in 3G. This transformation continues after 3G so that in 3I most of the precipitates are large θ'. Compared to 1I, the θ' in 3I has a smaller density and the individual plates are longer (larger) which is probably due to fewer θ' secondary platelets nucleating in the θ'' rich regions, so that each θ' draws solute from a larger volume.

On locus 4, as expected, less θ'' (if any) and secondary θ' can form upon ageing since more of the copper is already tied up. The θ' precipitates are fewer, larger, and thicker at 4G than at 1G or 3G. All misfit dislocations seen on the broad faces of θ' precipitates reflect incoherency and not preparation artifacts, since they appear in some micrographs where no other dislocations are visible. The SAD patterns in the ageing development of the number 4 panel material show very faint precipitate reflections, indicating that in general the amount of θ'' and θ' per unit volume is smaller than on loci 1 and 3. However, the sequence of streaks breaking into maxima remains. We avoided taking SAD patterns from big precipitates, so as not to skew the most representative patterns observed.

For the slowest cooled panel in each specimen from 7A to 7I, the formation of primary θ' and θ (upon cooling) dominates the character of the microstructure and properties. Some of the precipitates seen in 7A and 7I are extremely coarse, although thinner secondary θ' plates can be also seen in 7G, Fig. 3. The coarseness and the limited scope of secondary θ' precipitation indicate that most of the copper is taken to form θ' and θ during cooling. Therefore if a precipitation sequence $\theta'' \rightarrow \theta'$ exists, it does so only on a very restricted scale. Evidence for a $\theta'' \rightarrow \theta'$ transformation is shown by the SADP in 7G, Fig. 4, which exhibits streaks, maxima and {2 0 0} reflections. These details, however, were observed in only a small fraction of the areas viewed.

4. Discussion

The H–C response of the 2219 alloy upon ageing at 190° C and its dependence on microstructure can be discussed best by following the ageing locus 1 in Fig. 1 and comparing it to the microstructural evidence displayed in Figs. 3 and 4. While there is roughly a 50% increase in hardness between points A and D, caused by the precipitation of the coherent phases GP(1) and θ'', there is no significant change in conductivity. However, after the *HC* reversal where the dissolution of θ'' and the precipitation of θ' start, the hardness only decreases by about 9% between 1F and 1I, while the conductivity increases significantly, by 3.8 IACS units. The hardness behaviour is in excellent agreement with that reported by Rosen *et al.* [13] for a 5% stretched 2219 alloy aged at 175° C, but the explanation they give for the hardness and ultrasonic attenuation response is only partially borne out by our TEM observations. We find, as did they, that the increase in H when ageing starts is due to precipitation of the coherent phases GP(1) and θ'', but in our opinion the hardness peak and subsequent decrease on locus 1 is due more to the $\theta'' \rightarrow \theta'$ transformation itself than to loss of coherency of the θ'. There is no evidence in micrographs 1F to 1I for misfit dislocations indicating incoherency on the θ' precipitates. Furthermore, such incoherency is not expected to develop at 190° C ageing as shown in a study on a similar Al–Cu alloy by Foquet *et al.* [11]. Our results, in agreement with others [8, 11], seem at this point to indicate that it is the relative concentration of θ''- and θ'-phases, rather than loss of coherency, that leads to decreased hardness upon overageing, at temperatures below ca 200° C. It appears then that the first leg in the ageing sequence, the hardness rise, is a θ'' growth phenomenon. After the *HC* reversal, the second leg, the conductivity rise is a θ' growth phenomenon.

It has been claimed that while growing, the θ' precipitates drain most of the copper solute from the matrix, leading to a higher electrical conductivity [8]. Assuming this is true, the negligible change in C while θ'' grows from 1A to 1D indicates either that θ'' formation drains very little copper from the matrix, thereby leaving its conductivity unaffected, or that there is a copper drain, raising C, while the ordering of aluminium and copper in multilayers to form θ'' disturbs the lattice regularity, lowering C. These latter two events together may then balance each other resulting in a negligible net effect.

Two main trends in H–C develop when we go from locus 1 to 7; both basically reflect the increased precipitation of primary θ' and θ with

longer cooling times. First, in the as-quenched A specimens, the conductivity increases significantly from 1A to 7A, and this trend supports the model of the solute-lean matrix with higher conductivity. Second, the hardness drops dramatically over the same range. This drop is induced by the copper acquisition and increased incoherency of these first precipitates. The θ-phase is always incoherent, but the θ' precipitate coherency decreases from 3A to 7A as evidenced by increasing numbers of precipitates with misfit dislocations at their broad faces. The formation of solute-free regions around the θ' (and sometime θ) precipitates is illustrated in 3D, Figs. 3a and b. Since metastable, coherent GP(1) and θ'' do not form in these copper denuded regions, the increase in H before reaching each locus reversal becomes progressively smaller from 1 to 7. Moreover, loci 4 to 7 show a decrease in H at short ageing times, the reason for which is unclear. Once ageing starts, SAD indicates that the supersaturated $\alpha \rightarrow \text{GP}(1) \rightarrow \theta'' \rightarrow \theta'$ sequence is followed, contingent upon copper availability. The *HC* reversal always reflects the transfer from predominantly θ'' (or θ'' + primary θ') to only θ', and beyond it on each locus H decreases and C increases in accordance with the processes described on locus 1. While in absolute terms the drop in H between the reversal and point I is almost constant ($\sim$ 8 HRB) on all loci, the change in C decreases from 5.6 IACS units on locus 1 to 2 IACS units on locus 7. Since from 1A to 7A the major change in microstructure is the increase in the amount of primary θ' and θ, with a consequent copper-drain from the matrix before the ageing step, this reduced sensitivity of C to ageing also agrees well with the model of enhanced conductivity in a solute-lean matrix.

In summary, in the 2219 alloy, hardness depends mainly on the precipitate phase formed during quenching and is extremely sensitive to the first precipitates formed in an ageing sequence. In a fast-quenched material, the normal precipitation sequence: supersaturated $\alpha \rightarrow \text{GP}(1) \rightarrow \theta'' \rightarrow \theta'$ leads first to a large increase in H until the $\theta'' \rightarrow \theta'$ transformation occurs, and then to a slight decrease as θ' becomes the main phase. In a slower quenched material, precipitation of incoherent primary θ' and θ precipitates during cooling causes a markedly lower value in H before ageing starts. Upon ageing at 190° C, the rise of H is smaller and probably proportional to the amount of copper solute available for coherent θ'' precipitation. As in fast quenched materials, a further H-drop occurs after the transformation of θ'' to secondary θ'. Conductivity is mainly a function of the copper concentration in the matrix. It is not significantly affected by precipitation of the coherent phases GP(1) and θ'', but increases markedly with the drain of copper solute from the matrix by the formation of θ and/or θ'.

This work reinforces Chihoski's [1, 2] conclusion that the scatter in the H–C data reported by various researchers for the same alloy and nominal heat treatment mainly derive from process variations that lead to variations in the microstructure. Use of only H or only C to characterize the material is impossible, since the same hardness or conductivity can be found on materials with very different precipitate stati. However, the determination of the "sail" describing the field of H–C possibilities for any heat treatable aluminium alloy can provide an excellent reference for estimating the microstructure and the thermal history of a sample in a quick and nondestructive manner. Also, as an analytical device, it has the potential for revealing key precipitate conversions with high resolution, yet economically.

Acknowledgements

The authors want to thank Drs J. D. Venables, J. S. Ahearn, D. A. Hardwick, and L. Christodoulou for useful discussions in the course of this work.

References

1. R. CHIHOSKI, Proceedings of the DARPA Conference on Review of Progress in Quantitative NDE, San Diego, August 1982 (Plenum Publishing Co., 1982).
2. *Idem, Met. Prog.* **123** (6) (1963) 27.
3. E. HORNBOGEN, *Aluminium* **43** (1967) 164.
4. R. B. NICHOLSON and J. NUTTING, *Phil. Mag.* **3** (1958) 531.
5. H. YOSHIDA, D. J. H. COCKAYNE and M. J. WHELAN, *ibid.* **34** (1976) 89.
6. A. GUINIER, *J. Phys. Radium* **8 (iii)** (1942) 124.
7. V. A. PHILLIPS, *Acta Metall.* **23** (1975) 751.
8. L. SWARTZENDURBER *et al.*, NBS Report NBSIR 80-2069, December 1980.
9. C. LAIRD and H. I. AARONSON, *Acta Metall.* **14** (1966) 121.
10. G. C. WEATHERLY and R. B. NICHOLSON, *Phil. Mag.* **17** (1968) 801.
11. F. FOUQUET, P. MERLE, M. KOHEN, J. MERLIN and P. F. GOBIN, *Acta Metall.* **27** (1979) 315.
12. J. M. PAPAZIAN, *Met. Trans. A* **12A** (1981) 269.
13. M. ROSEN, E. HOROWITZ, S. FICK, R. C. RENO and R. MEHRABIAN, *Mater. Sci. Eng.* **53** (1982) 163.

Received 15 February
and accepted 7 March 1983